Doppler-free two-photon spectroscopy in the vacuum ultraviolet: helium 1^1S-2^1S transition

S. D. Bergeson

Department of Physics and Astronomy, Brigham Young University, Provo, Utah 84602-4640

K. G. H. Baldwin

Research School of Physical Sciences and Engineering, Australian National University, Canberra, ACT 0200, Australia

T. B. Lucatorto

National Institute of Standards and Technology, Gaithersburg, Maryland 20899-0001

T. J. McIlrath

American Physical Society, One Physics Ellipse, College Park, Maryland 20740-3844

C. H. Cheng and E. E. Eyler

University of Connecticut, Department of Physics, 2152 Hillside Road, Storrs, Connecticut 06269-3046

Received December 21, 1999; revised manuscript received May 15, 2000

We describe techniques for laser spectroscopy in the vacuum-UV (VUV) spectral region that combine high spectral resolution with high absolute accuracy. A nearly transform-limited nanosecond laser source at 120 nm is constructed with difference-frequency mixing. This source is used to perform the first, to our knowledge, Doppler-free VUV measurement. We measure the inherently narrow 1^1S-2^1S two-photon transition in atomic helium with a spectral resolution of 7 parts in 10^8 (180 MHz), the narrowest line width so far observed at such short wavelengths. Careful measurements of optical phase perturbations allow us to determine the absolute frequency of the line center to a fractional uncertainty of 1 part in 10^8. Improvements now in progress should reduce this uncertainty to 2 parts in 10^9. © 2000 Optical Society of America [S0740-3224(00)01009-2]

OCIS codes: 020.5580, 300.6210, 300.6360, 190.4380, 140.3610, 300.6540.

1. INTRODUCTION

New narrow-band laser sources in the far-UV and vacuum-UV (VUV) spectral regions are important not only because of the present paucity of such lasers but also because this is the spectral range of the primary resonance transitions in most atoms and small molecules. We developed an intense and well-characterized laser source near 120 nm, using four-wave mixing, for use in precision two-photon spectroscopy of atomic helium (He). Although our own application is to fundamental atomic physics, narrow-bandwidth VUV laser radiation is also needed for numerous other applications. Obvious examples include spectroscopy of small molecules, for which high resolution is needed to resolve the rotational and vibrational structure, and optical processes requiring highly coherent radiation, such as adiabatic population transfer by means of stimulated Raman adiabatic passage.

In the far-UV region remarkable progress has been made in recent years. Among the most impressive achievements of modern precision spectroscopy is the measurement of the hydrogen $1s-2s$ forbidden transition with ever-increasing accuracy.[1] This two-photon transition near 242 nm was recently measured with a fractional uncertainty of 1.5×10^{-14}. Measurements of this kind provide determinations of the Rydberg constant,[2] the proton size,[3,4] and test quantum electrodynamics calculations in simple systems.[5]

In the VUV region the technical obstacles are much more difficult. High-accuracy Doppler-reduced spectroscopic measurements on He at 58 nm have been demonstrated.[6–8] Prior to our recent research[9,10] Doppler-free spectroscopic techniques had been employed successfully only at wavelengths greater than 191 nm, the cutoff for producing VUV radiation by frequency mixing in crystals of β-barium borate (BBO). We describe here some of the technical details involved in our recent measurement of the He 1^1S-2^1S transition, using two-photon excitation at 120.28 nm.[9,10] The He measurement and its significance were described in our prior pub-

lications. Here we describe the generation and characterization of transform-limited VUV laser radiation, together with some of the practical considerations involved in performing accurate two-photon spectroscopy at such a short wavelength. The He resonance transition has several highly desirable attributes: It is a two-photon transition and therefore can be measured Doppler free; the long 20-ms lifetime of the upper state results in a natural linewidth of only 8 Hz[11–13]; and this long lifetime allows for detection of the resonance by an ionizing laser delayed by many times the pulse duration, thus eliminating any Stark shifts arising from the ionizing pulse. The main challenges in using this transition are generating sufficient narrow-band VUV power to drive the transition (there is no resonant enhancement) and performing accurate metrology to determine the absolute frequency of the transition.

Ideally, we would like to excite the He transition with a continuous-wave (cw) laser source. Unfortunately, cw sources at 120 nm did not exist at all until recently, and at present only ~0.5 nW of output power can be attained.[14] Far higher powers are needed for two-photon excitation, requiring us to use a pulsed system. Our VUV generation is based on four-wave difference-frequency mixing (4WDFM) of a pulse-amplified cw laser and its harmonics. To account for the optical phase perturbations inherent in such pulsed amplification and upconversion, we use an optical heterodyne technique to measure the perturbation of the optical phase during pulse amplification.

2. FOUR-WAVE DIFFERENCE-FREQUENCY MIXING IN KRYPTON

Coherent VUV radiation can be generated with a number of different methods, including harmonic upconversion,[6–8,15] sum–difference-frequency generation,[16–18] stimulated Raman scattering,[19] and others.[20–28] Of these techniques, 4WDFM is perhaps the most versatile. It has an advantage over harmonic and sum-frequency generation of providing continuous-wavelength coverage because of its ability to phase match appropriately for both positive and negative wave-vector mismatch.[29] In addition, the use of favorable two-photon resonances enables efficient conversion over much of the VUV. This is to be compared with stimulated Raman scattering, for which the efficiency decreases with increasing anti-Stokes order, owing both to the nonlinearity of the process and to the increasing dispersion of typical Raman shifting media at short wavelengths.[30] 4WDFM is also less affected by Stark broadening of the laser bandwidth than stimulated Raman scattering, for which high powers are required for overcoming the low efficiencies and the need to operate well above threshold.[19]

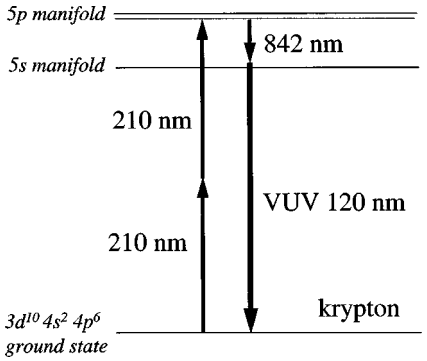

Fig. 1. 4WDFM VUV generation scheme in Kr employed in the present experiment. The gray horizontal line represents a virtual state.

For the purpose of measuring the He 1^1S-2^1S transition frequency using two-photon spectroscopy, we need a VUV source at 120 nm. Figure 1 shows frequency mixing in krypton (Kr) for a near-infrared laser (at 842 nm) and its fourth harmonic (at 210 nm). The 210-nm radiation (with an energy of 47,508 cm^{-1}) is nearly two-photon resonant with the $4p^5 5p$ manifold ($5p[1/2]_{J=0}$, $\Delta\sigma = +923$ cm^{-1}, and $5p[3/2]_{J=2}$, $\Delta\sigma = +1892$ cm^{-1}),[31] where $\Delta\sigma$ is the difference between the photon energies and the Kr energy levels. A single photon at 842 nm is difference-frequency mixed to an energy at 83,139 cm^{-1} (120.28 nm), which is near resonant with the $4p^5 5s$ manifold ($5s[3/2]_{J=1}$, $\Delta\sigma = +2221$ cm^{-1}, and $5s'[1/2]_{J=0}$, $\Delta\sigma = -2054$ cm^{-1}). The VUV radiation can be tuned over the required range ($\ll 1$ cm^{-1}) without significantly affecting the phase-matching or resonant-enhancement parameters.

Much higher efficiency could be attained by use of two lasers with slightly differing frequencies. This would enable us to tune the 210-nm radiation much closer to resonance with the appropriate Kr levels. However, the 4WDFM scheme outlined above has a high enough efficiency for the present experiment, and the increased VUV production in this case does not compensate for the additional complication of measuring the absolute frequency of two pulsed lasers. A detailed calculation of the VUV intensity required for driving the He 1^1S-2^1S transition is reported in Ref. 10.

3. PULSE-AMPLIFIED 842-nm LASER AND HARMONICS

The high-resolution, high-power laser used to generate the fundamental 842-nm radiation is shown schematically in Fig. 2. A cw-injected pulse-amplifier system provides the nearly Fourier-transform-limited radiation required for high-resolution measurements.

We inject approximately 300 mW of single-frequency radiation from a Ti:sapphire laser at 842 nm into a five-stage dye amplifier system. A 650-mJ/pulse 532-nm Nd:YAG laser pumps the amplifier chain. The pump laser is itself injection locked by a cw laser to provide a temporally smooth envelope of 7-ns duration and a high spatial beam quality. This is important for creating a nearly Fourier-transform-limited bandwidth and for optimizing the nonlinear conversion efficiency. It is also important for minimizing shot-to-shot fluctuations in the optical phase excursions.[32]

The output of the second amplification stage is spatially filtered before final amplification by three longitudinally pumped amplifier stages. Using lenses (not

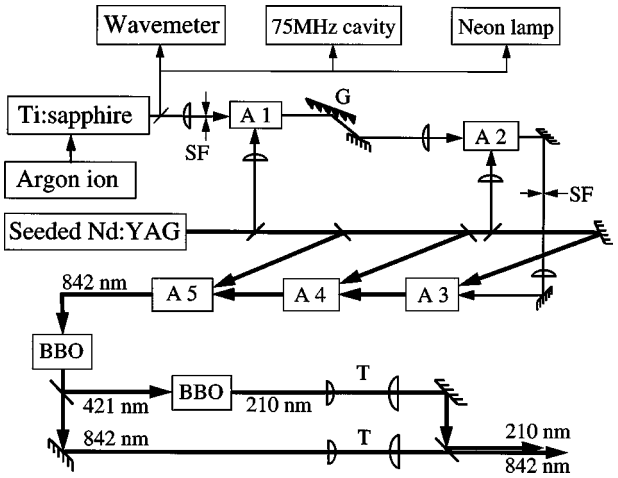

Fig. 2. Pulse-amplified dye laser and frequency multiplication scheme used to generate the fundamental (842-nm) and the fourth-harmonic (210-nm) input wavelengths for the VUV generation process. A, amplifier; G, grating; SF, spatial filter; T, telescope.

shown in Fig. 2), we relay image the pump laser output onto the final two longitudinal amplifiers. This dramatically improves the spatial quality of the 842-nm beam, which is crucial for high-efficiency harmonic upconversion. The amplifier chain produces up to 50 mJ at 842 nm.

The fourth harmonic at 210 nm is generated by means of frequency doubling twice in BBO crystals. Typical pulse energies in the second harmonic (410 nm) and the fourth harmonic (210 nm) are 10 and 2 mJ, respectively. After the first BBO crystal, a dichroic mirror separates the 421- and the 842-nm beams and diverts the 421-nm radiation into the second BBO crystal. After the second BBO crystal and before the telescope, two UV-grade fused-silica prisms (not shown) are used in a minimum-deviation arrangement for spatial separation of the 421- and the 210-nm radiation.

The 842- and the 210-nm radiation are combined on a dichroic mirror and directed into the four-wave mixing cell. Before the beams are recombined, a separate telescope in each beam expands the beams to 1-cm diameter and then focuses them to a point at the center of the cell. Because the efficiency of 4WDFM depends nonlinearly on the laser intensity, a tight focus in the cell enhances VUV production. One of the lenses in the 210-nm telescope is on a translating stage. The stage, in addition to other mirror adjustments, allows for *in situ* optimization of the 210- and the 842-nm focal spot overlap in the x, y, and z axes inside the cell.

4. OPTIMIZING VACUUM-ULTRAVIOLET PRODUCTION

4WDFM is performed in a stainless-steel cell filled with Kr gas, as shown in Fig. 3. The cell is separated from our main vacuum chamber by a MgF_2 lens. The efficiency of the 4WDFM process is measured with nitric-oxide (NO) ionization to detect the 120-nm radiation.[33] To measure the VUV production efficiency, the main vacuum chamber is filled with NO at a pressure of 133 Pa (1.0 Torr). The NO gas is ionized by the VUV radiation. The resulting photocurrent is collected by a pair of metal plates (10 cm long, parallel to the VUV beam), one of which is held at a potential of −70 V. With the laser running at 10 Hz, we measured a photocurrent of 35–45 nA, corresponding to a pulse energy of approximation 50 nJ.

The relatively high conversion efficiency (50 nJ/2 mJ $= 2.5 \times 10^{-5}$) in this mixing scheme is achieved by addition of argon to the Kr to enhance the phase matching. A plot showing the relative VUV production for different Kr/argon (Ar) ratios is shown in Fig. 4. For the experiment we use a 4:1 volume ratio Kr/Ar mixture with a total pressure of 33 kPa (250 Torr). We fill the 4WDFM cell, using separate gas cylinders for the Kr and the Ar. The time for these gases to mix thoroughly is relatively long, so we use a small circulation pump to mix the gases briefly after filling the cell.

One final comment on the NO detector is that we measure a series of strong ionization signal peaks from the 210-nm radiation, depending on the exact wavelength. This signal appears when the 210-nm radiation resonantly populates a level in the NO molecule, which is then ionized by a second 210-nm photon. It is therefore important (and simple) when measuring the 120-nm signal to choose a wavelength at which this extraneous signal is absent.

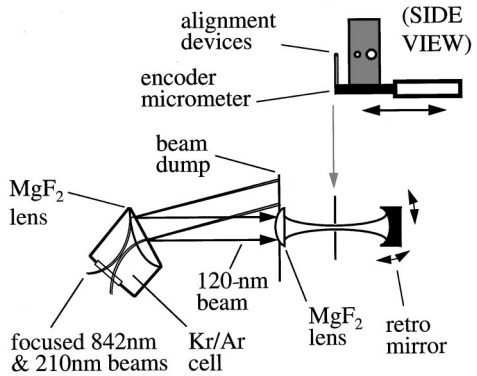

Fig. 3. Optical arrangement for the VUV generation system, including a side view of alignment devices (inset).

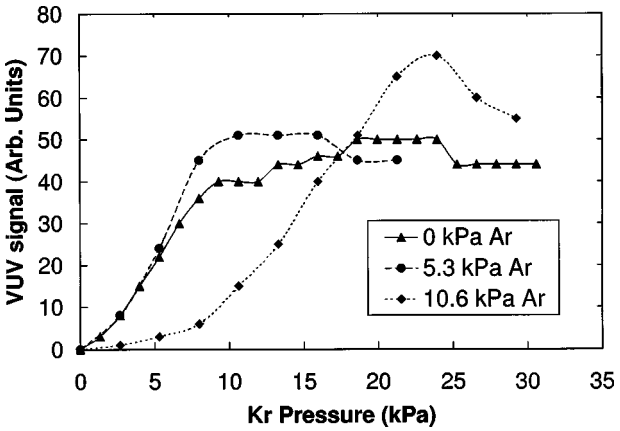

Fig. 4. VUV signal output as a function of Kr and Ar pressure used in the phase-matching process.

5. VACUUM-ULTRAVIOLET OPTICAL SYSTEM

Our optical system is designed with the He spectroscopy measurements in mind. At 120 nm it is important to use as few optical elements as possible, because of the relatively poor transmission of most materials. For the He two-photon 1^1S-2^1S spectroscopy, for which the transition rate scales as the intensity squared, a high-efficiency optical system is crucial. Our design minimizes the number of optical elements, provides high rejection of unwanted wavelengths, and maintains a high-quality spatial mode in the VUV radiation. Eliminating unwanted wavelengths in the interaction region reduces ac-Stark shifts in our measurements to a negligible level. Maintaining a high-quality spatial mode allows for tight focusing of the VUV radiation in the interaction region, further increasing the He transition rate.

The output window of the 4WDFM cell is a tilted, off-axis MgF_2 lens (30-cm focal length at 120 nm; see Fig. 3). It is positioned such that light exiting the cell strikes the curved front surface at normal incidence, collimating the VUV radiation. The flat back surface of the lens lies at an angle with respect to the propagation vector and provides prismlike dispersion of the 842-, 210-, and 120-nm beams. Approximately 45 cm after the tilted lens an aperture blocks the longer-wavelength beams, passing only the 120-nm radiation. A second MgF_2 lens (30-cm focal length at 120 nm) just after the aperture focuses the radiation into a high-density supersonic He expansion.[34] This second lens is mounted on a motorized $x-y-z$ translation stage, allowing for some adjustability in the focal position. A concave MgF_2-coated aluminum mirror with 12.7-mm diameter and 12.7 mm focal length placed after the He expansion reflects and reimages the focal spot back on top of itself, in a standard Doppler-free arrangement—two counterpropagating plane-parallel radiation fields. We measure the reflective efficiency of this mirror to be 68% at 120 nm.

Because all transmissive optics exhibit large dispersion in the VUV region, the proper alignment is wavelength sensitive and can be made *in vacuo* only at 120 nm. For the alignment we fix the center of curvature of the concave mirror in the center of the He expansion. The alignment task is then reduced to placing the VUV focus at that same point. Using a closed-loop translation stage, we place a small prealigned aperture (ϕ=0.5 mm) at the center of curvature of the concave mirror and adjust the position of the second MgF_2 lens to maximize the VUV transmission through the pinhole. This aperture is then removed and replaced with a smaller aperture ($\phi = 0.05$ mm) centered at the same height on the translation stage driven by the precision encoder. Again the position of the focusing lens is adjusted to optimize the VUV transmission through the aperture, and then this second aperture is removed. This alignment procedure is close enough to produce a small Doppler-free signal. Finally, the lens position is adjusted to optimize the Doppler-free signal.

For the supersonic He expansion we use a stagnation pressure of 2×10^5 Pa and maintain a pressure in the vacuum system of less than 1.3×10^{-3} Pa (10^{-5} Torr). The focal point of the second MgF_2 lens is located 15 mm from the He nozzle. We measure the line-integrated density across the 10-mm-long confocal interaction region to be 3×10^{14} cm^{-3}.

Each step in the upconversion process temporally compresses the laser pulse. Considering the degree of saturation of different steps in the process, we estimate the VUV pulse duration to be ~3 ns. If we assume a ~50% transmission of second lens, the peak VUV power in the interaction region is 10 W.

We measure the diameter of the focus, using a sharp knife edge on a motorized stage with a closed-loop actuator. The knife edge is electrically isolated from ground and connected to an electrometer. We measure the VUV-induced photocurrent while stepping the knife across the beam to determine the beam diameter (40 μm). The resulting VUV intensity (8×10^5 W/cm^2) is more than adequate to drive the two-photon transition.[10]

6. RESONANCE DETECTION

Following two-photon excitation by the 120-nm radiation, the He 2^1S level is ionized by the frequency-quadrupled output from a second Nd:YAG laser (30 mJ in a 7-ns pulse at 266 nm) as shown in Fig. 5. The ionizing laser is introduced through a port at 45° to, and in the same plane as, the VUV and the He beams. A 300-mm-focal-length cylindrical quartz lens loosely focuses the 266-nm radiation to create a high-intensity ionizing beam at the center of the interaction region with near-unity ionizing efficiency[35] (see Fig. 6). The ionizing pulse is delayed 30 ns relative to the 120-nm pulse to prevent Stark shifting of the He energy levels by the high-intensity ionizing laser pulse.

The He ions are collected and counted by the time-of-flight mass spectrometer (TOFMS) shown in Fig. 6. The TOFMS consists of a pair of oppositely charged extraction plates to remove the ions from the interaction region, following which they enter a field-free region 150 mm long. The flight times produced by this method yield excellent

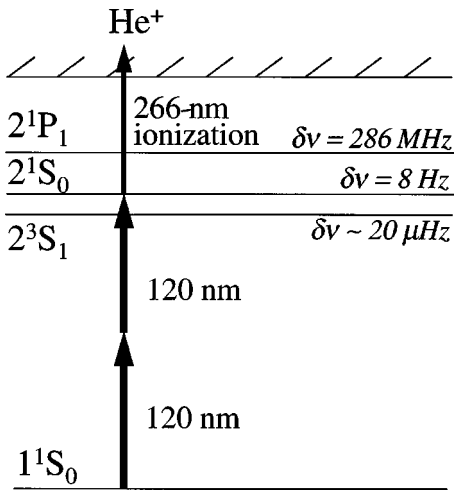

Fig. 5. He energy level diagram showing the excitation and ionization scheme for the 1^1S-2^1S transition.

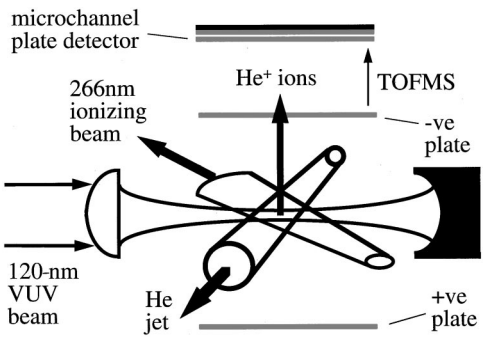

Fig. 6. Interaction region for the Doppler-free two-photon resonant, three-photon ionization process.

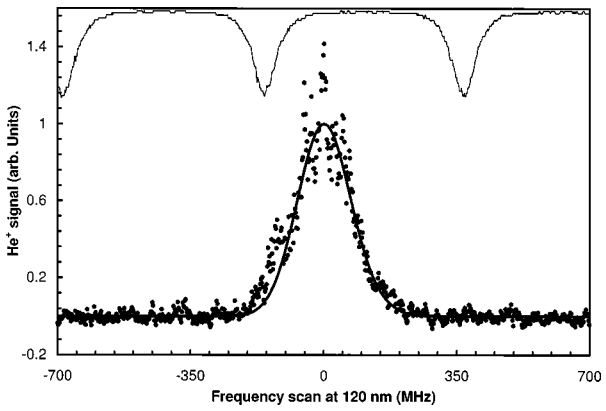

Fig. 7. Detailed spectrum of the Doppler-free portion of the He^+ signal (circles) averaged over three scans. Also shown is a least-squares fit to the data (bottom curve) and the inverted reference etalon signal (top).

discrimination for the He signal over nearby impurity species. The He ions then collide with a microchannel plate that acts both as a detector and an amplifier.

Figure 7 shows an average of three scans over the Doppler-free component of the He 1^1S-2^1S transition at 120 nm. At the center of the line we count approximately 50 ions per laser pulse. The He signal is smoothed with a 3-s time constant and sampled at 10 Hz. The natural width of the He 1^1S-2^1S transition is only 8 Hz. Therefore the observed width of the transition in Fig. 7 indicates the spectral width of the VUV radiation. The observed transition width at 120 nm is 180 MHz.

7. LASER METROLOGY

In a pulse-amplified laser system the instantaneous frequency in the pulse is not necessarily the same as the cw laser source. Optical phase perturbations during pulse amplification can result in significant frequency deviations during the pulse evolution. Therefore we measure the 120-nm wavelength in three steps. First we measure the wavelength of the cw laser at the center of the He 1^1S-2^1S signal. Second, we determine the instantaneous pulsed-laser frequency at 842 nm relative to the cw laser source. Finally, we determine the additional phase perturbations introduced in the harmonic upconversion process.

A. Measuring the Continuous-Wave Laser Wavelength

The absolute value for the He two-photon transition frequency is measured by determination of the 842-nm cw laser frequency with reference to a neon (Ne) transition 8 GHz away (at 11,877 cm^{-1}) which serves as a wavelength transfer standard. This particular Ne line is difficult to see in absorption, because the lower level of the transition is not metastable. We observe the transition in a Doppler-free saturated absorption spectrometer, as shown in Fig. 8. A few milliwatts of 842-nm radiation are directed through the positive column discharge. The discharge lamp is filled with ^{20}Ne at a pressure of 133 Pa (1.0 Torr) and operated at a dc current of 6.6 mA. The discharge is confined by a 350-mm-long, 2-mm-diameter capillary.

Using a passively stabilized confocal etalon with a 75-MHz free spectral range, we measure the frequency separation between the He and the Ne transitions by counting the number of transmission fringes produced as the fundamental cw laser is scanned rapidly between the two lines. An example of such a scan is shown in Fig. 9. Here the He transition on the left-hand side appears as a sharp Doppler-free line superimposed over a broad, Doppler-broadened pedestal. The Doppler-free Ne line appears likewise on the right-hand side of the figure. In between, 107 fringes with 75-MHz spacing define the 8-GHz separation between the two lines.

The position of the Ne reference transition in this particular discharge lamp is determined with respect to an iodine-stabilized 633-nm He–Ne laser in a separate experiment.[9]

B. Optical Pulse Perturbations in Pulsed Amplification

During the phase-amplification process some of the coherence of the cw laser source is lost. Some loss of coherence is inevitable, owing to the pulse nature of the output. The spectral bandwidth cannot be any narrower than the Fourier transform of the laser pulse.

An additional loss of coherence comes from optical frequency perturbations during the pulse-amplification process. In our experiment the cw laser passes through a series of dye cells. The gain of the medium depends on the dye molecule excited-state population, which changes dramatically over the evolution of the pulse from the pumping laser (the Nd:YAG laser). When the gain changes, so does the index of refraction, as well as the linear susceptibility of the medium. These changes directly

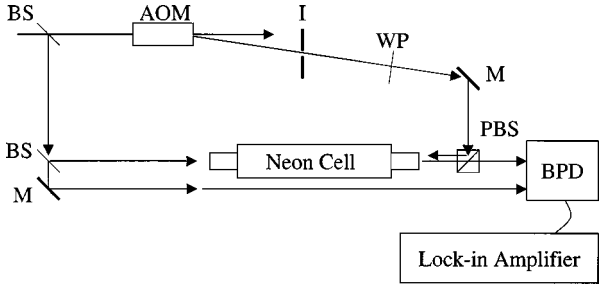

Fig. 8. Schematic diagram of the Ne absorption spectrometer: BS, beam splitter; AOM, acousto-optic modulator; WP, wave plate; M, mirror; PBS, polarizing beam splitter; BPD, balanced photodiode.

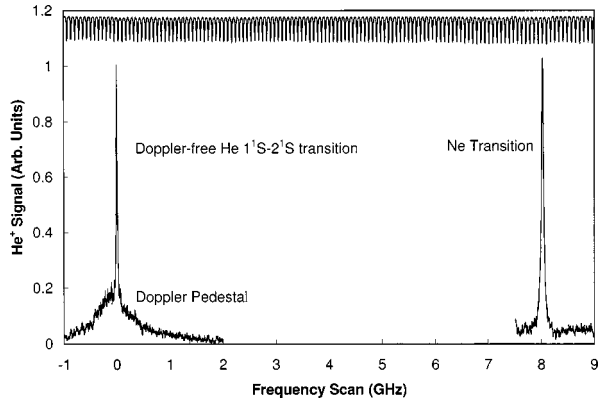

Fig. 9. Spectrum of the complete He transition (left-hand side) and the Ne reference line (right-hand side) as a function of cw (842-nm) laser detuning. Also shown is the inverted output signal from the 75-MHz reference cavity.

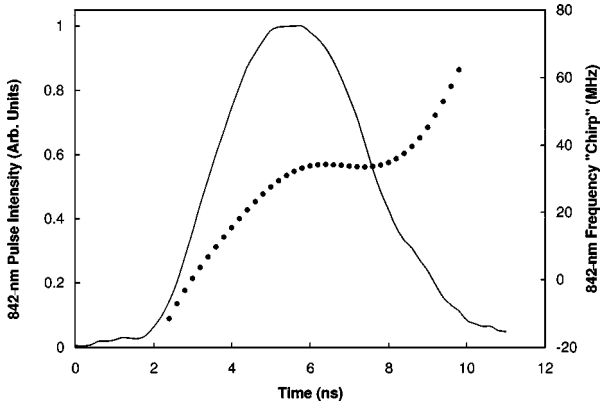

Fig. 10. Instantaneous frequency of the pulsed laser (circles) as a function of time. For reference the intensity of the 842-nm laser pulse is also plotted (curve) on the same time scale.

influence the instantaneous optical phase of the pulse, which is related to the instantaneous optical frequency.

Considerable progress has been made in recent years for accurate characterization of these perturbations and also for minimizing their magnitude. Using an improved version of the optical heterodyne technique first demonstrated by Fee *et al.*[36] we measure the perturbation of the optical phase during pulse amplification. From this measurement we derive the instantaneous frequency and predict the two-photon line shape. Adjusting only the center frequency and the amplitude of the model line shape, we fit the model to the observed signal and determine the two-photon transition frequency.

Our heterodyne technique is described in detail in Refs. 10, 32, and 37. In brief, a portion of the cw beam is shifted 400 MHz by an acousto-optic modulator. This cw beam is mixed with a portion of the fully amplified pulsed beam on a fast photodiode. This produces a 400-MHz beat note inside the pulse envelope. The beat note is Fourier analyzed to determine the instantaneous optical phase, which is then differentiated to determine the instantaneous frequency. Figure 10 shows the instantaneous frequency of the 842-nm laser during the laser pulse. The frequency changes most rapidly during the rising and falling edge of the pulse. Because the harmonic upconversion and 4WDFM processes are nonlinear in the laser intensity, the frequency behavior in the highest-intensity regions of the laser pulse is most important. Across the FWHM of the laser pulse the frequency change is modest. The frequency shift is relatively stable and reproducible and approximately 25 MHz higher in frequency than the cw laser. The fractional uncertainty in reconstructing the optical phase of the laser pulse before harmonic upconversion is 6×10^{-9} and after harmonic upconversion is 1×10^{-8}. For a detailed discussion of the optical phase measurement the reader is referred to Refs. 10, 32, and 37.

C. Optical Phase Perturbations in Four-Wave Difference-Frequency Mixing

A discussion of optical phase perturbations during frequency doubling is found in Ref. 32. Optical phase perturbations arising from the 4WDFM process are difficult to estimate. In our experiment we measure the apparent frequency of the He 1^1S-2^1S transition frequency as a function of the 210-nm pulse energy. We determine the phase perturbations from the 4WDFM process by plotting the shift of the apparent transition frequency with power and correct them to lowest order by extrapolating to zero pulse intensity.

A plot of the apparent transition frequency versus 210-nm pulse energy is shown in Fig. 11. Each point in the figure is an average of five separate measurements at the indicated pulse energy. The vertical error bars reflect the 1σ statistical scatter in all the data points at the indicated pulse energy, summed in quadrature with the random uncertainties associated with reconstructing the optical phase. The horizontal error bars represent the uncertainty in the power measurements. We find that the 1^1S-2^1S transition energy appears to shift at a rate of approximately -85 MHz/mJ. Because this is a two-photon transition, the frequency shift at 120 nm as a function of 210-nm pulse energy is therefore approximately -43 MHz/mJ.

D. Error Budget

The above uncertainties are summarized in Table 1. For consistency all uncertainties are given in terms of their

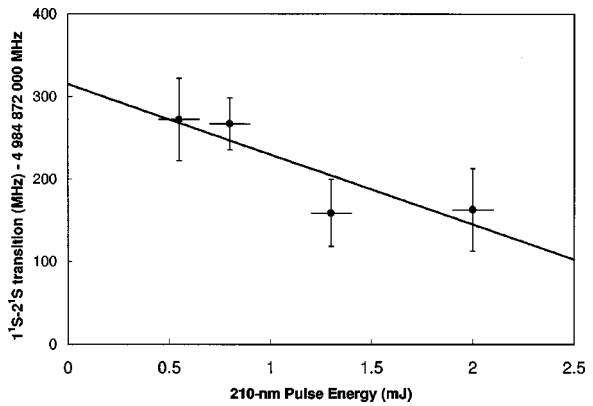

Fig. 11. Plot of the apparent frequency of the He 1^1S-2^1S transition as a function of 210-nm pulse energy. The slope of this line is -85 MHz/mJ. This translates into a shift at 120 nm of -43 MHz/mJ.

Table 1. Uncertainty Budget for He 1^1S-2^1S Transition[a]

Source	Uncertainty (MHz)
ac Stark shift	0.7
Ne reference transition	5.6
Free spectral range	6.3
Frequency scan	10.0
Optical phase perturbation	13.0
Zero power extrapolation	44.0
Combined standard uncertainty	48
	1 part in 10^8

[a] The transition energy is 4 984 872 315 MHz.

contribution to the 1^1S-2^1S transition energy. Doppler-free spectroscopy cancels the first-order Doppler shift, and the second-order Doppler shift is negligible. The peak intensity in the interaction region in the Doppler-free arrangement is 10^6 W/cm^2, giving a worst-case ac Stark shift of 0.7 MHz. The Ne calibration uncertainty contributes 5.6 MHz. The uncertainty in the Fabry–Perot free spectral range contributes 6.3 MHz. The possible error stemming from nonlinearity in the cw laser frequency scan between the He and the Ne lines is no larger than 10 MHz. We estimate that the systematic uncertainty in processing the optical phase perturbation contributes 13 MHz.

The largest contribution to the error budget is the possible phase perturbation in the harmonic upconversion process (see Subsection 7.C and Fig. 11). The error in determining the slope of the fit to the data in Fig. 11 contributes 44 MHz to the 1^1S-2^1S transition energy.

The combined standard uncertainty from all these sources is 48 MHz. As reported in Ref. 9, the He 1^1S-2^1S transition energy measured with this laser system is 4 984 872 315±48 MHz. For a more detailed discussion on how this measurement is used to determine the ground-state Lamb shift, and for a comparison with theory and other experiments, the reader is referred to Refs. 6–10.

8. DISCUSSION AND FUTURE RESEARCH

Improving the accuracy of pulsed-laser spectroscopy is probably best pursued by means of developing sources with reduced overall optical phase perturbations and developing methods for more accurately characterizing the instantaneous VUV frequency. It has been shown that the proper mixture of dye solution in dye amplifier systems can dramatically reduce the overall optical phase perturbation.[32]

Another method of compensating for the optical phase perturbations during pulse amplification of a cw source was used by Eikema *et al.*[38] Using a fast algorithm, they determined the instantaneous frequency of their laser pulse and used an electro-optic modulator to put the *negative* of the frequency excursion on the cw laser. This imprinted frequency excursion is then nearly canceled during the pulse-amplification process. This so-called antichirping method was demonstrated in the fifth-harmonic generation of a frequency-doubled 584-nm laser. In this way the fractional width of the laser was reduced to 1.1×10^{-7}.

A longer pulse duration in the pump laser will also decrease the magnitude of the perturbations. In a longer (Gaussian-shaped) pulse the rising edge of the pulse is less steep. This results in a slower transfer of populations in the dye sample and a smaller overall optical phase perturbation. An improved version of the laser system under development at the University of Connecticut includes a long-pulse injection-seeded Nd:YAG laser.

With a more accurately characterized 842-nm pulse it should be easier to predict the two-photon transition line shape with high fidelity. This would allow us to examine carefully the additional optical phase perturbations arising from the 4WDFM process. With this approach it seems possible to reduce the fractional uncertainty in the absolute frequency determination from 1×10^{-8} to a few times 10^{-9}.

Recently, a 0.5-nW cw laser source at 120 nm was demonstrated.[14] It may be possible in some future experiment to use a cw source to measure the He 1^1S-2^1S transition with much higher accuracy. However, present cw sources appear to be less than ideal. Modifying our previous calculation of the two-photon transition rate,[10] we can find the expected excitation rate for the best currently available cw 120-nm laser source. For 1 nW at 120 nm, 1-MHz line width, focused to a 20-μm Gaussian waist in 0.1-Torr He gas, with a 2-cm confocal parameter, the expected excitation rate to the 2^1S metastable state is approximately 1 atom per 1000 s. An optical buildup cavity could be used to increase the intensity in the interaction region. However, the best mirrors to our knowledge have a reflectivity of ~85%,[39] implying a maximum buildup of ~6.7. This increases the excitation rate to one atom every 20 s. A future cw experiment of this kind requires a substantially brighter VUV source or substantially improved VUV optics.

ACKNOWLEDGMENTS

We thank other contributors to this long-term project, especially Ashok Balakrishnan, Jon Marangos, Tom O'Brian, Steve Rolston, Craig Sansonetti, Jesse Wen, and Natalie Westbrook.

This research was supported by the National Institute of Standards and Technology, the University of Connecticut, the National Research Council, the National Science Foundation (NSF), and the NSF/Australian Department of Industry, Science and Resources Collaborative Grants Scheme.

S. Bergeson's e-mail address is scott.bergeson @byu.edu.

REFERENCES

1. A. Huber, B. Gross, M. Weitz, and T. W. Hänsch, "High-resolution spectroscopy of the $1S-2S$ transition in atomic hydrogen," Phys. Rev. A **59**, 1844–1851 (1999).
2. B. de Beauvoir, F. Nez, L. Julien, B. Cagnac, F. Biraben, D. Touahri, L. Hilico, O. Acef, A. Clairon, and J. J. Zondy, "Absolute frequency measurement of the $2S-8S/D$ transitions

in hydrogen and deuterium: new determination of the Rydberg constant," Phys. Rev. Lett. **78**, 440–443 (1997).
3. K. Pachucki, D. Leibfried, M. Weitz, A. Huber, W. König, and T. W. Hänsch, "Theory of the energy levels and precise two-photon spectroscopy of atomic hydrogen and deuterium," J. Phys. B **29**, 177–195 (1996).
4. K. Pachucki, "Quantum electrodynamics effects on singlet S-states of helium of order $m\alpha^6$," J. Phys. B **31**, 3547–3556 (1998).
5. P. J. Mohr, "Quantum electrodynamics calculations," in *The Spectrum of Hydrogen: Advances*, G. W. Series, ed. (World Scientific, New York, 1988), p. 111.
6. K. S. E. Eikema, W. Ubachs, W. Vassen, and W. Hogervorst, "First laser excitation of the ^{4}He 1^1S-2^1P resonance line at 58 nm," Phys. Rev. Lett. **71**, 1690–1692 (1993).
7. K. S. E. Eikema, W. Ubachs, W. Vassen, and W. Hogervorst, "Precision measurements in helium at 58 nm: ground state Lamb shift and the 1^1S-2^1P transition isotope shift," Phys. Rev. Lett. **76**, 1216–1219 (1996).
8. K. S. E. Eikema, W. Ubachs, W. Vassen, and W. Hogervorst, "Lamb shift measurement in the 1^1S ground state of helium," Phys. Rev. A **55**, 1866–1884 (1997).
9. S. D. Bergeson, A. Balakrishnan, K. G. H. Baldwin, T. B. Lucatorto, J. P. Marangos, T. J. McIlrath, T. R. O'Brian, S. L. Rolston, C. J. Sansonetti, J. Wen, N. Westbrook, C. H. Cheng, and E. E. Eyler, "Measurement of the He ground state Lamb shift via the two-photon 1^1S-2^1S transition," Phys. Rev. Lett. **80**, 3475–3478 (1998).
10. S. D. Bergeson, A. Balakrishnan, K. G. H. Baldwin, T. B. Lucatorto, J. P. Marangos, T. J. McIlrath, T. R. O'Brian, S. L. Rolston, C. J. Sansonetti, J. Wen, N. Westbrook, C. H. Cheng, and E. E. Eyler, "Precision spectroscopy in He as a test of QED," Phys. Scr. T **83**, 76–82 (1999).
11. G. W. F. Drake, G. A. Victor, and A. Dalgarno, "Two-photon decay of the singlet and triplet metastable states of helium-like ions," Phys. Rev. **180**, 25–32 (1969).
12. R. S. Van Dyck, Jr., C. E. Johnson, and H. A. Shugart, "Radiative lifetime of the 2^1S_0 metastable state of helium," Phys. Rev. A **4**, 1327–1336 (1971).
13. V. Jacobs, "Two-photon decay rate of the 2^1S_0 metastable state of helium," Phys. Rev. A **4**, 939–944 (1971).
14. K. S. E. Eikema, J. Walz, and T. W. Hänsch, "Continuous wave coherent Lyman-α radiation," Phys. Rev. Lett. **83**, 3828–3831 (1999).
15. K. G. H. Baldwin, J. P. Marangos, and D. D. Burgess, "Application of coherent VUV radiation to the measurement of Lyman-α absorption lineshapes in a dense Z-pinch plasma," J. Phys. D **17**, L169–L173 (1984).
16. J. P. Marangos, N. Shen, H. Ma, M. H. R. Hutchinson, and J. P. Connerade, "Broadly tunable vacuum-ultraviolet radiation source employing resonant enhanced sum-difference frequency mixing in krypton," J. Opt. Soc. Am. B **7**, 1254–1263 (1990).
17. N. Melikechi, S. Gangopadhyay, and E. E. Eyler, "Generation of vacuum ultraviolet radiation for precision laser spectroscopy," Appl. Opt. **36**, 7776–7778 (1997).
18. P. M. Dooley, B. R. Lewis, S. T. Gibson, K. G. H. Baldwin, P. C. Cosby, J. L. Price, R. A. Copeland, T. G. Slanger, A. P. Thorne, K. Yoshino, and J. E. Murray, "A comparative high-resolution study of predissociation linewidths in the Schumann–Runge bands of O_2," J. Chem. Phys. **109**, 3856–3867 (1998).
19. B. R. Lewis, S. T. Gibson, K. G. H. Baldwin, and J. H. Carver, "Vacuum-ultraviolet absorption linewidth measurement using high-order anti-Stokes Raman-shifted radiation," J. Opt. Soc. Am. B **6**, 1200–1208 (1989).
20. C. R. Vidal, "Coherent VUV sources for high resolution spectroscopy," Appl. Opt. **19**, 3897–3903 (1980).
21. W. Jamroz and B. P. Stoicheff, "Generation of tunable coherent vacuum ultraviolet radiation," in *Progress in Optics*, E. Wolf, ed. (North-Holland, Amsterdam, 1983), p. 325.
22. R. Hilbig, G. Hilber, A. Lago, B. Wolff, and R. Wallenstein, "Tunable coherent VUV radiation generated by nonlinear optical frequency conversion in gases," Comments At. Mol. Phys. **18**, 157–180 (1986).
23. C. R. Vidal, "Vacuum ultraviolet laser spectroscopy of small molecules," Adv. At. Mol. Phys. **23**, 1–35 (1988).
24. M. N. R. Ashfold and J. D. Prince, "Multiphoton processes in molecular gases," Contemp. Phys. **29**, 129 (1988).
25. A. Lago, "Generation of VUV/XUV laser light," AIP Conf. Proc. **225**, 29–34 (1991).
26. J. W. Hepburn, "Applications of coherent vacuum ultraviolet to photofragment and photoionization spectroscopy," in *Vacuum Ultraviolet Photoionization and Photodissociation of Molecules and Clusters*, C. Y. Ng, ed. (World Scientific, Singapore, 1991), Chap. 9, pp. 435–485.
27. K. Yamanouchi and S. Tsuchiya, "Tunable vacuum ultraviolet laser spectroscopy: excited state dynamics of jet-cooled molecules and van der Waals complexes," J. Phys. B **28**, 133–165 (1995).
28. R. Hilbig and R. Wallenstein, "Narrowband tunable VUV radiation generated by nonresonant sum- and difference-frequency mixing in xenon and krypton," Appl. Opt. **21**, 913–917 (1982).
29. G. C. Bjorklund, "Effects of focusing on third-order nonlinear processes," IEEE J. Quantum Electron. **QE-11**, 287–296 (1975).
30. K. G. H. Baldwin, J. P. Marangos, D. D. Burgess, and M. C. Gower, "Generation of tunable coherent VUV radiation by anti-Stokes Raman scattering of excimer-pumped dye laser radiation," Opt. Commun. **52**, 351–354 (1985).
31. C. E. Moore, "Atomic energy levels," National Standard Reference Data System–National Bureau of Standards 35 (U.S. Government Printing Office, Washington, D.C., 1971), Vol. 1.
32. S. Gangopadhyay, N. Melikechi, and E. E. Eyler, "Optical phase perturbations in nanosecond pulsed amplification and second-harmonic generation," J. Opt. Soc. Am. B **11**, 231–241 (1994).
33. J. Samson, *Vacuum Ultraviolet Techniques* (Wiley, New York, 1967).
34. T. A. Miller, "Chemistry and chemical intermediates in supersonic free jet expansions," Science **223**, 545–553 (1984).
35. T. N. Chang and T. K. Fang, "Effect of positive-energy orbitals on the photoionization cross sections and oscillator strengths of He and divalent atoms," Phys. Rev. A **52**, 2638–2644 (1995).
36. M. S. Fee, K. Danzmann, and S. Chu, "Optical heterodyne measurement of pulsed lasers: toward high-precision pulsed spectroscopy," Phys. Rev. A **45**, 4911–4923 (1992).
37. N. Melikechi, S. Gangopadhyay, and E. E. Eyler, "Phase dynamics in nanosecond pulsed dye laser amplification," J. Opt. Soc. Am. B **11**, 2402–2411 (1994).
38. K. S. E. Eikema, W. Ubachs, W. Vassen, and W. Hogervorst, "Lamb shift measurement in the 1^1S ground state of helium," Phys. Rev. A **55**, 1866–1884 (1997).
39. Acton Research Corporation, aluminum mirror with a MgF_2 coating.